View metadata, citation and similar papers at core.ac.uk

brought to you by CORE

provided by Lehigh University: Lehigh Preserve

Lehigh University
Lehigh Preserve

Theses and Dissertations

1-1-1979

Design study of a lidar system for close range distance measurement.

John R. Regazzi

Follow this and additional works at: http://preserve.lehigh.edu/etd


Part of the Electrical and Computer Engineering Commons

Recommended Citation
Regazzi, John R., "Design study of a lidar system for close range distance measurement." (1979). *Theses and Dissertations.* Paper 1877.

This Thesis is brought to you for free and open access by Lehigh Preserve. It has been accepted for inclusion in Theses and Dissertations by an authorized administrator of Lehigh Preserve. For more information, please contact preserve@lehigh.edu.

DESIGN STUDY OF A LIDAR SYSTEM FOR CLOSE RANGE DISTANCE MEASUREMENT

by

John R. Regazzi

A Thesis

Presented to the Graduate Committee

of Lehigh University

in Candidacy for the Degree of

Master of Science

in

Electrical Engineering

Lehigh University

1979

ProQuest Number: EP76149

All rights reserved

INFORMATION TO ALL USERS
The quality of this reproduction is dependent upon the quality of the copy submitted.

In the unlikely event that the author did not send a complete manuscript
and there are missing pages, these will be noted. Also, if material had to be removed,
a note will indicate the deletion.

ProQuest EP76149

Published by ProQuest LLC (2015). Copyright of the Dissertation is held by the Author.

All rights reserved.
This work is protected against unauthorized copying under Title 17, United States Code
Microform Edition © ProQuest LLC.

ProQuest LLC.
789 East Eisenhower Parkway
P.O. Box 1346
Ann Arbor, MI 48106 - 1346

CERTIFICATE OF APPROVAL

This thesis is accepted and approved in partial fulfillment of the requirements for the degree of Master of Science in Electrical Engineering.

5/2/79
(date)

Professor in Charge

Chairman of Department

Acknowledgements

I wish to thank Professor Nikolai Eberhardt for the good experience gained from working with him. I would also like to thank Professor Bruce Fritchman for his generous help.

Table of Contents

Abstract

The principal system parameters of a short range Lidar device for accurate distance measurements in the range of a few meters are theoretically and experimentally studied. The system operates with a 4 GHz-CW-modulation and is intended for dimensional measurements in industrial production.

After outlining the proposed system, some of its basic components, such as modulators, are experimentally investigated. A first working setup of the essential parts is reported and discussed. Theoretical estimates are presented for the roundtrip attenuation, expected accuracy and speed of measurement.

Introduction

Accurate measurements of distance may be accomplished optically by techniques employing the comparison of phase between a carrier and its echo. Although relative displacements of .1μm are measurable[1], this type of interferometry requires that the reflected beam preserves its coherent nature. For this purpose a retroreflector must normally be affixed to the target since light scattered from a diffuse surface will, generally, not be spatially coherent. In addition, lateral movements of the target surface will produce an effective loss of temporal coherence as well[2].

To circumvent this difficulty, modern ranging systems typically incorporate modulation of beam intensity[3]. While some systems have been developed using light emitting diodes, certain advantages result when the source is coherent. Distance is determined by measuring the phase shift in the modulation signal upon its return from the target. Such systems can operate without a retroreflector, however, maximum target range is restricted for low power beams.

In this paper the feasibility of a short range system that will not require a retroreflector is investigated. The arrangement employs as high a modulating frequency as possible in order to maximize distance resolution. 4 GHz has been chosen as the highest frequency that can be handled with reasonable effort and

expense.

System Description

Because the microwave modulation is not easily detected directly, frequency translation is performed at the receiver by heterodyning with a second microwave signal of slightly different frequency. The phase remains unaffected by mixing and thus distance information is preserved. Our initial setup, shown schematically in Figure 1A, uses a 2 mW linearly polarized He-Ne gas laser as the source. The beam was polarization modulated using the Pockels effect[4] in $LiTaO_3$. A polarizer following the crystal, oriented crossed to that of the laser, provides overall intensity modulation. The focusing lens represents an attempt to thread the beam through the modulator.

The transmitted beam is focused to a spot on a target at approximately 3 meters distance with the aid of a beam expander. Reflecting tape, used for initial measurements, was later replaced with a diffuse reflector. A telescope receiver is indispensable as the returned beam will be severely attenuated. Also, the scattered light must be refocused through a second modulator for the purpose of demodulation. The final system will incorporate an optical reference path to compensate the effects of added phase shifts due to temperature changes. This arrangement will require a double crystal modulator design so that two beams can be demodulated simultaneously. Our equipment, however, employed an elec-

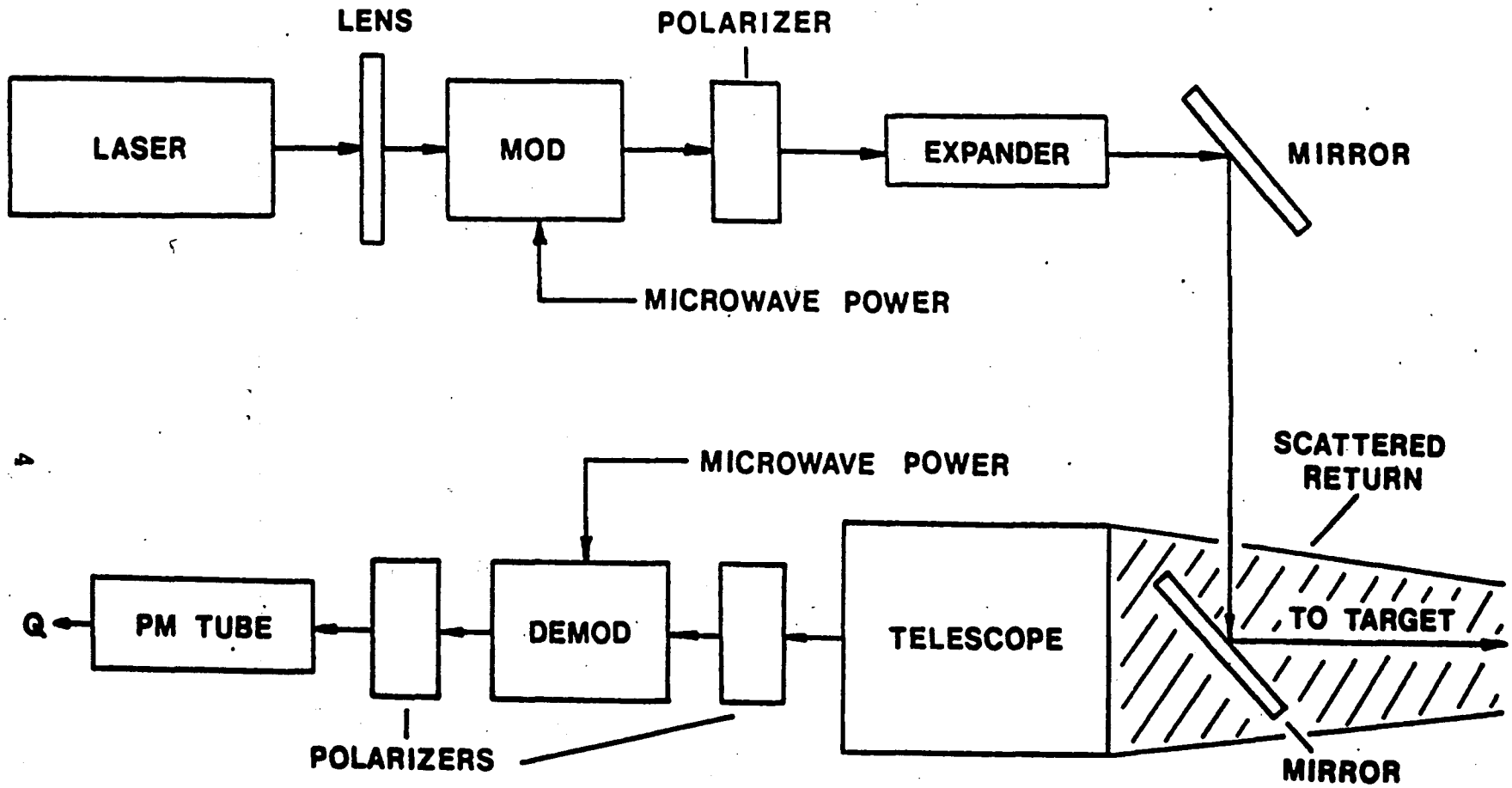

FIGURE 1A A functional block diagram of the LIDAR system showing the principle light path.

trical reference derived by direct mixing of the modulating and demodulating frequencies.

Two stable microwave transistor oscillators were used for modulation and demodulation. Separate traveling wave tube amplifiers were able to provide 1 watt of power each at 4 GHz. One of the transistor oscillators was modified to provide frequency adjustment by means of a tuning screw. IF frequencies as low as 3 KHz were possible with this arrangement. Detection is accomplished with a photomultiplier tube, chosen for its high sensitivity and low noise. The tube produces a current, at the IF frequency, proportional to the incident light power. Distance is calculated from the phase difference between this signal and the reference mentioned earlier. Feasible resolution is a small fraction of the modulating wavelength. A photograph of an initial laboratory setup is given in Figure 1B.

Modulators

The Pockels effect in $LiTaO_3$[4] has been used to affect polarization modulation of a coherent laser source. The properties of birefringent crystals are such that, within the crystal, only two waves with mutually orthogonal directions of polarization are allowed in a given direction of propagation. The theory of polarization modulation[5] requires linearly polarized light to be incident on the crystal in a direction oriented 45 degrees from either of the internally allowed directions.

FIGURE 1B A photograph of the initial laboratory setup. Note the Lissajous pattern visible at the top, giving the phase in the scattered light.

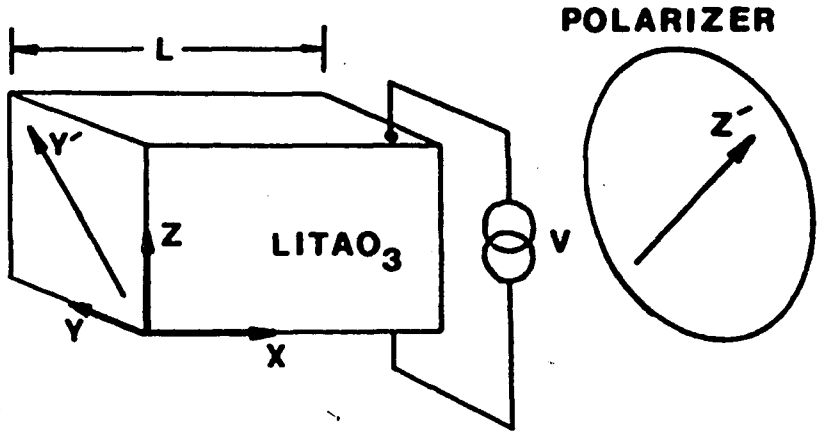

FIGURE 2 A transverse electrooptic modulator using $LiTaO_3$.

The crystal is cut in such a way as to make the allowable directions of polarization, with light propagating in the x direction, equal to the y and z axes as shown in Figure 2 (z is the direction of the optic axis). If N_0 represents the power of the incident light wave whose polarization is along y', then the components of the electric field within the crystal can be written as

$$E_y = \frac{1}{\sqrt{2}} E_{y'} \text{ and } E_z = \frac{1}{\sqrt{2}} E_{z'} e^{j\Gamma}$$

or

$$E_y = \sqrt{\frac{N_0}{2}}\, e^{j\omega_\ell t} \text{ and } E_z = \sqrt{\frac{N_0}{2}}\, e^{j(\omega_\ell t + \Gamma)} \qquad (1)$$

where ω_ℓ represents the light frequency and Γ represents the phase difference between the two waves. This phase term is necessary because each wave, while inside the crystal, propagates at a different velocity dictated by the anisotropy of the crystal structure. This velocity difference gives rise to an increasing phase difference as the two waves propagate through the crystal. The amount of phase shift accumulated can be altered by application

of an external electric field parallel to the optic axis. This is known as the transverse electrooptic effect because the modulating field is applied normal to the direction of propagation. For this reason a modulator making use of the transverse electrooptic effect has the advantage of an unobstructed optical path.

The two separate waves will recombine upon leaving the crystal, producing a composite wave whose polarization will depend upon the phase index Γ. Thus, the polarization of the emerging beam can be modulated with the applied electric field. Modulation of the polarization can be transformed into intensity modulation by placing a linear polarizer immediately following the crystal. Optimum performance is achieved when the preferred direction of the analyzer is 90 degrees from the laser's direction of polarization. From Figure 2, the analyzer output would be given by $E_{z'}$ and after a suitable rotation of coordinates can be written as

$$E_{z'} = \sqrt{\frac{N_o}{2}}\, e^{j\omega_\ell t} \cdot \frac{1}{\sqrt{2}} - \sqrt{\frac{N_o}{2}}\, e^{j\omega_\ell t}\, e^{j\Gamma} \cdot \frac{1}{\sqrt{2}}$$

or

$$E_{z'} = \frac{N_o}{\sqrt{2}} e^{j\omega_\ell t}\ (1 - e^{j\Gamma}) \qquad (2)$$

If a transmission ratio S is defined as

$$S = \frac{\text{available output intensity}}{\text{available input intensity}} \qquad (3)$$

then S represents a static modulation curve for the modulator and illustrates how changes in phase effects output intensity. This ratio can be expressed as

$$S = \left[\frac{E_{z'}}{E_{y'}}\right]\left[\frac{E_{z'}}{E_{y'}}\right]^{*}$$

or $$S = \frac{1}{2}(1 - e^{j\Gamma}) \cdot \frac{1}{2}(1 - e^{j\Gamma})$$

$$S = \sin^2\left(\frac{\Gamma}{2}\right) \qquad (4)$$

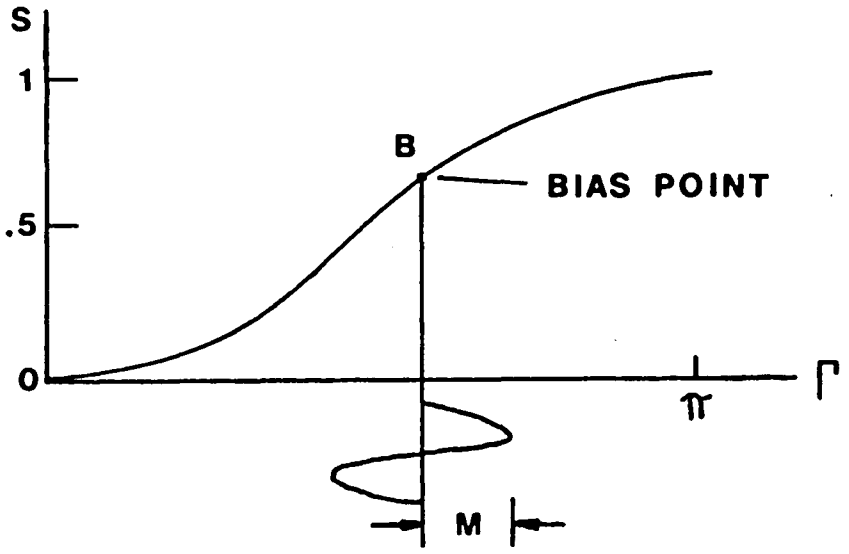

FIGURE 3 The static modulation curve for the electrooptic intensity modulator.

Referring to the static modulation curve plotted in Figure 3, two new parameters will be defined. The first is the operating point B, often called the natural birefringence of the crystal. This refers to the phase shift induced when the applied electric field is zero. In practice, however, the operating point can be adjusted with the application of a dc field. The addition of an ac field will alternately aid and cancel the dc field and thus it

is useful to define the quantity m as the peak deviation from the bias point B. In this way the phase index Γ may be written as

$$\Gamma = m \sin \omega_m t + B \tag{5}$$

where ω_m is the modulating frequency. Although modulation sensitivity increases with crystal length, transit time effects[5] will degrade performance if the crystal is made too long. It is interesting to note, however, that transit time effects do not influence the shape of the static modulation curve, even though less modulation is achieved with a given voltage. A complete discussion of the principles of electrooptic modulation can be found in the books of either Yariv [5] or Harvey[6], (see also [8])

The swing factor m is an appropriate indicator of modulator performance for two reasons. First, m is linearly related to the electric field strength within the crystal. This relationship can serve as a procedural check by plotting measured values of m against modulating voltage. Secondly, m is a direct measure of the modulation depth achieved and becomes helpful when making relative comparisons between modulators. The crystal is usually biased at $\pi/2$ to provide the most linear modulation and for this case alone it is convenient to define a modulation index μ. Consider the equation for the instantaneous amplitude of a general linear AM carrier, given by

$$A(t) = A_c\left[1 + \mu f_n(t)\right] \tag{6}$$

where $f_n(t)$ is the normalized modulating signal and A_c is the carrier amplitude. From (4) and (5) it follows that the normalized instantaneous power transmitted by the modulator can be expressed as

$$S = \sin^2\left(\frac{M}{2}\sin(\omega_m t) + \frac{B}{2}\right) \tag{7}$$

For a bias at $\pi/2$ equation (7) can be expressed in the form of (6) yielding

$$S = 1/2\left(1 + \sin(m \sin \omega_m t)\right) \tag{8}$$

or for values of $m << 1$

$$S = 1/2\ (\ 1 + m \sin \omega_m t\ ) \tag{9}$$

Under these restrictions the swing factor and the modulation index are interchangeable. If the condition $m << 1$ is not fulfilled, an approximate expression for μ can be obtained by expanding $\sin(m \sin \omega_m t)$ as

$$\sin(m \sin \omega_m t) = 2\ J_1(m) \sin \omega_m t + 2\ J_3(m) \sin 3\omega_m t + 2\ J_5(m) \sin 5\omega_m t + \cdots$$

Neglecting harmonic terms, equation (8) becomes

$$S = 1/2\ (\ 1 + 2\ J_1(m) \sin \omega_m t\ ) \tag{10}$$

The modulation index is now given by

$$\mu = 2\, J_1(m) \qquad (11)$$

It is felt that by this approach, μ best reflects the saturation effects of the static modulation curve.

When the modulator is biased at zero, the variation in carrier intensity will occur at twice the modulating frequency. The advantage of this mode of operation is the potential to increase the system resolution. Unfortunately, the amplitude of the variation in carrier intensity suffers, and in general, this mode of operation will require more modulating power. Because performance data are not available for this case, the analysis will be restricted to the linear mode of operation (i.e. bias at $\pi/2$).

The arrangement of Figure 4 was used to measure the swing factor m.

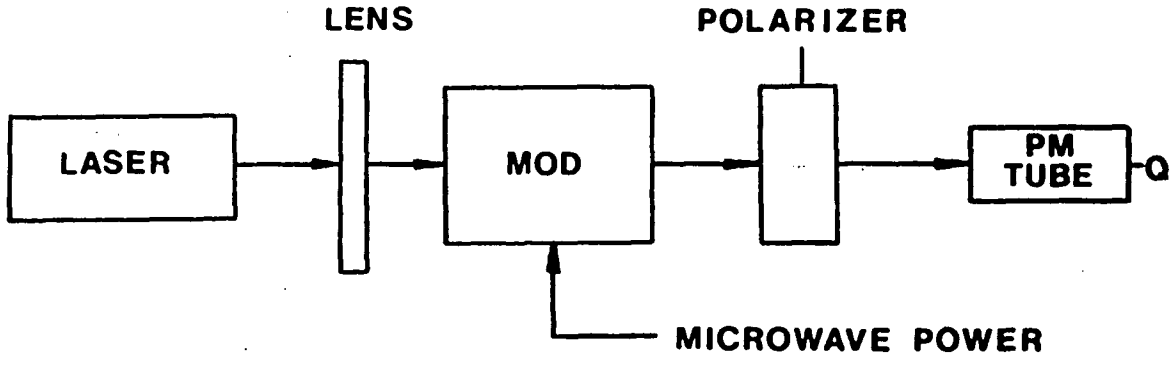

FIGURE 4 The detector is placed immediately following the transmitter so that modulator performance can be determined.

Unfortunately, a photomultiplier tube cannot respond to intensity variations more rapid than about 400 MHz. Therefore, m must be assessed indirectly by noting average changes in carrier intensity. If Q denotes the photodetector output, then

$$Q = \frac{1}{T}\int_0^T S\, dt \tag{12}$$

where T is the period of S. Substituting (7) into (12) and simplifying yields

$$Q = 1/2\left\{1 - \frac{\cos B}{T}\int_0^T \cos(m \sin \omega_m t)\ dt + \frac{\sin B}{T}\int_0^T \sin(m \sin \omega_m t)\, dt\right\} \tag{13}$$

For any integer number of cycles the second integral will be zero because the sin is an odd function. The first integral over the same period is identically the zeroth order Bessel function of m. Thus, the final expression for Q becomes

$$Q = 1/2\left(1 - \cos B \cdot J_0(m)\right) \tag{14}$$

The curves of Figure 5 represent how the detector output will change with bias point for various levels of applied modulating power. Thus, verification of the static modulation curve can be accomplished by measuring the photomultiplier current at various bias points while the microwave power is off. By repeating this procedure when the microwave power is on, estimation of m is possible from (14). It was found that when modulating power is

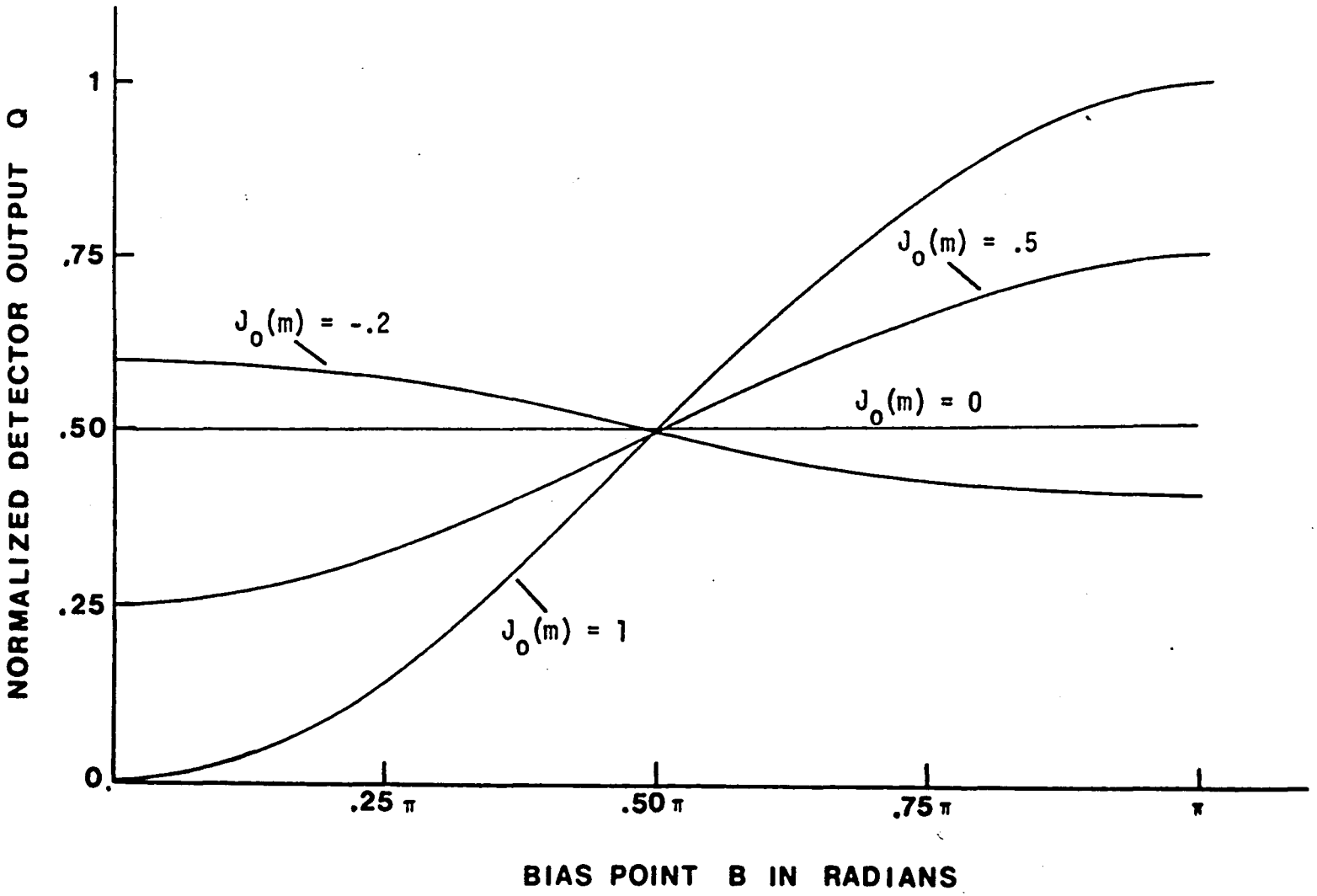

FIGURE 5 Detector output verses bias point for various swing factors.

applied, the bias point shifts appreciably and this can be attributed to the thermal sensitivity of the natural birefringence of $LiTaO_3$. Table I shows the detector output measured at various bias points while pulsing the microwave power; a 10-percent duty cycle adequately avoided heating of the crystal. With this technique, the modulation curve and the swing factor can be measured simultaneously.

TABLE I

Bias Voltage Referred to B = 0	DETECTOR OUTPUT IN ARBITRARY UNITS	
	Microwave power Off	Peak microwave Power = .94 watts
0	0	4
50	3	6
100	7	10
150	15	16
200	25	23
250	34	30
300	37	34
350	40	36

The data of Table I are shown graphically in Figure 6 to allow comparison with the predicted curves of Figure (5). The swing factor is found to be .92 rad or 82-percent intensity modulation for a power input of .94 watts. This shows an efficiency compar-

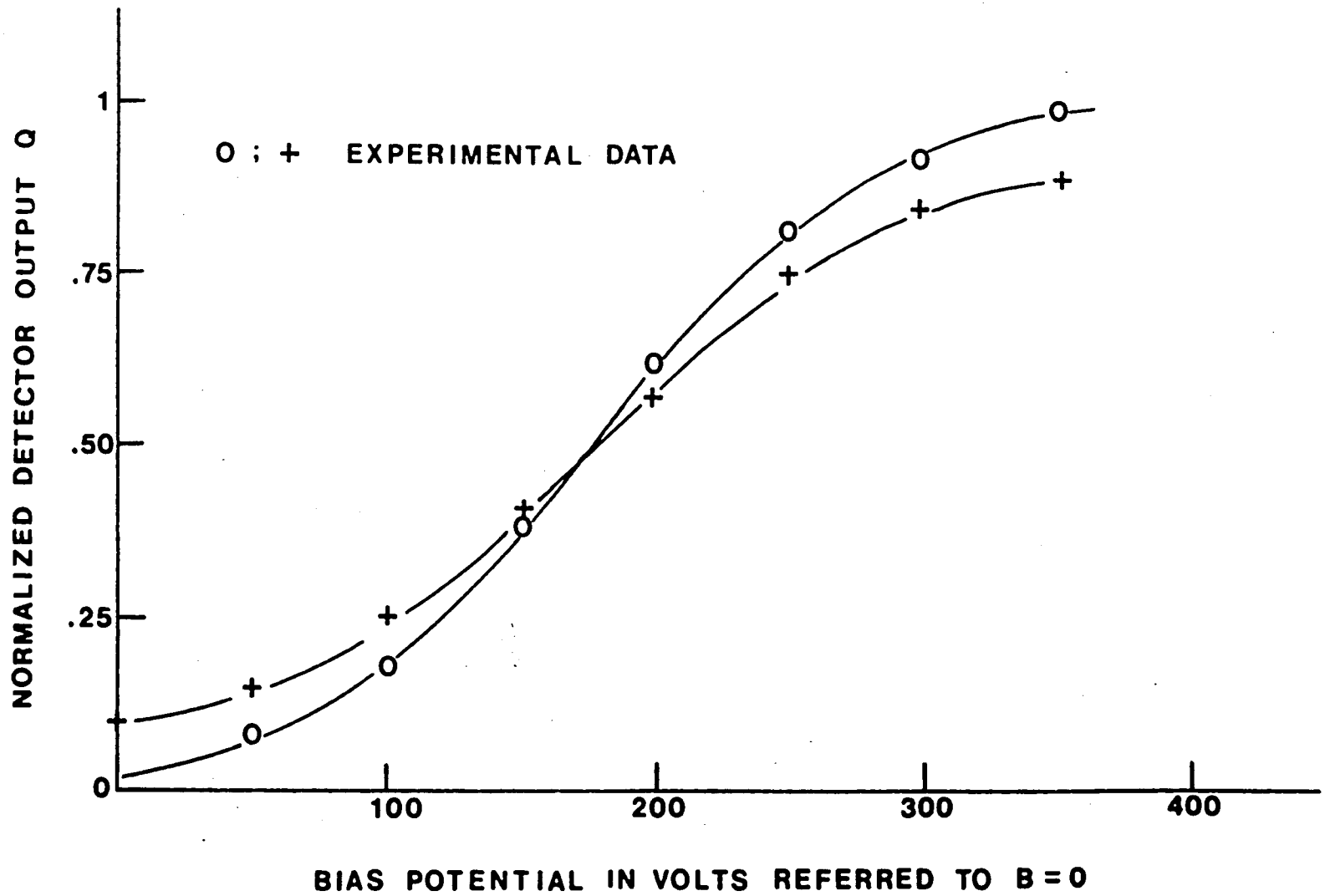

FIGURE 6 Measured performance of reentrant cavity modulator.

able with the previous results of Kaminov and Sharpless[7]. A similar reentrant microwave cavity was employed in which the $LiTaO_3$ is supported in a way that maximizes the electric field within the crystal. However, the cavity design precludes application of a dc field and thus a separate crystal is required to provide bias adjustment. While two crystals can be arranged so that temperature effects are minimized, increased beam attenuation is unavoidable. Clearly, a modulator design using only one crystal is more desirable.

Demodulation

The purpose of modulating the received light with a second microwave signal is to produce a low frequency component. It follows from the modulation theorem that the spectrum of the photomultiplier current will contain a component at the difference frequency. If N_i/N_o represents the normalized instantaneous light power incident on the photocathode, then from (10) it follows that

$$\frac{N_i}{N_o} = \frac{A_t}{4} (1 + \mu \sin \omega_1 t)\cdot(1 + \mu \sin \omega_2 t) \qquad (15)$$

where the subscripts refer to the modulating and demodulating frequencies and A_t is the transmission attenuation. Here, the same modulation index μ is assumed in both modulators. If the photomultiplier and associated circuitry is assumed to act as a low pass filter with a bandwidth $<< \omega_1$ or ω_2, then by ex-

panding (15) and retaining those terms within the passband, the normalized instantaneous power available for detection can be written as

$$\frac{\hat{n}_i}{N_o} = \frac{A_t}{4}\left(1 + \frac{\mu^2}{2}\cos\left(\omega_1 - \omega_2\right) t\right) \tag{16}$$

where an IF modulation index can be considered as

$$\mu_{IF} = \mu^2/_2 \tag{17}$$

The swing factor m was measured at various power levels using the technique previously described. The factors μ and μ_{IF}, obtained from (11) and (17) respectively, are shown in Figure 7 plotted against microwave power. The IF modulation index will approximately be linearly related to the modulating power since the swing factor is directly proportional to voltage. With 100-percent modulation in each modulator, the IF index is 50-percent.

Round Trip Attenuation

Beam scattering at the target and depth focus limitations are the two considerations most responsible for degrading the received signal to noise ratio. The two $LiTaO_3$ crystals within each modulator are arranged as shown in Figure 8.

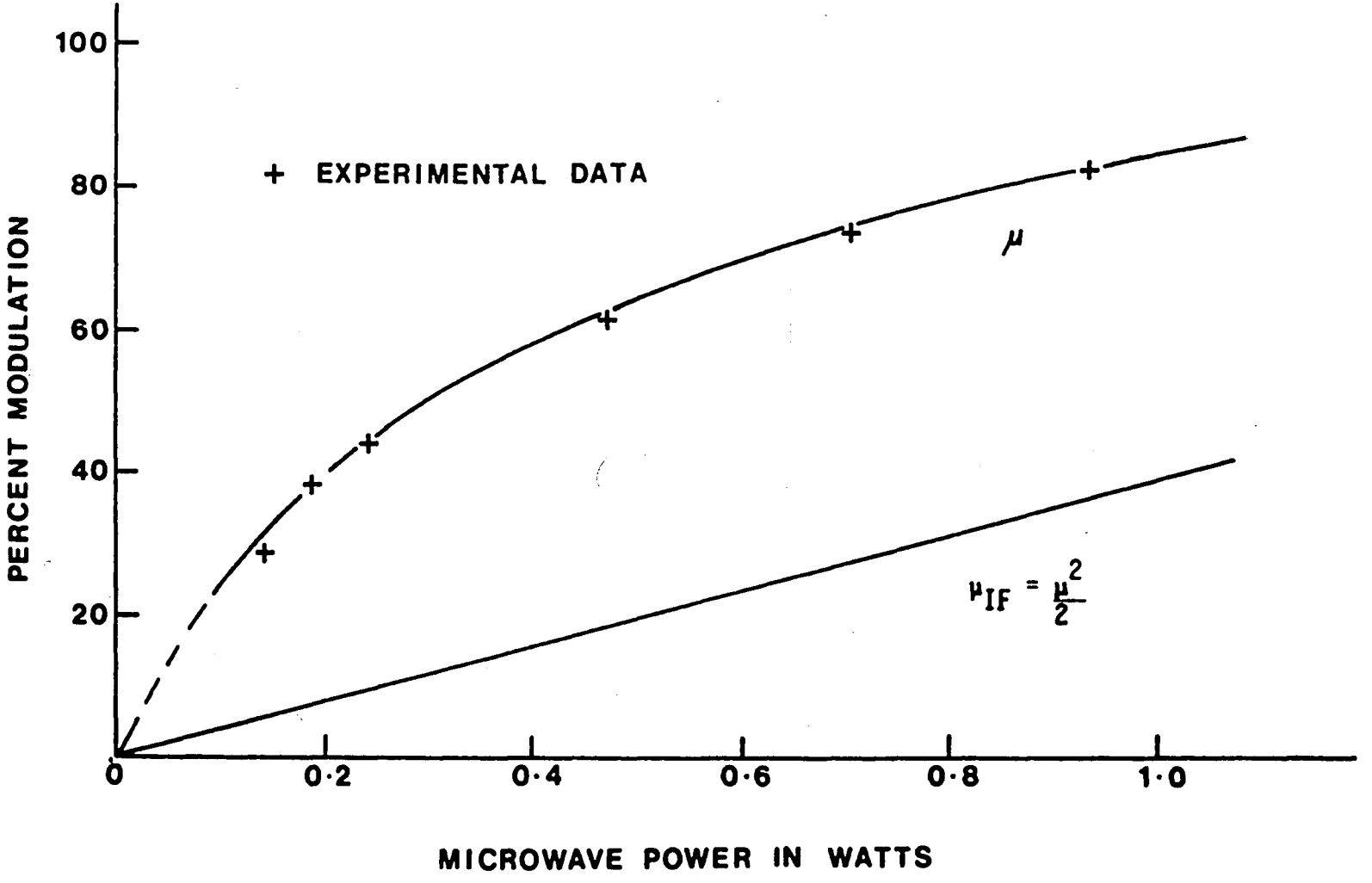

FIGURE 7 Measured performance of reentrant cavity modulator. The IF modulation index will saturate at 50-percent.

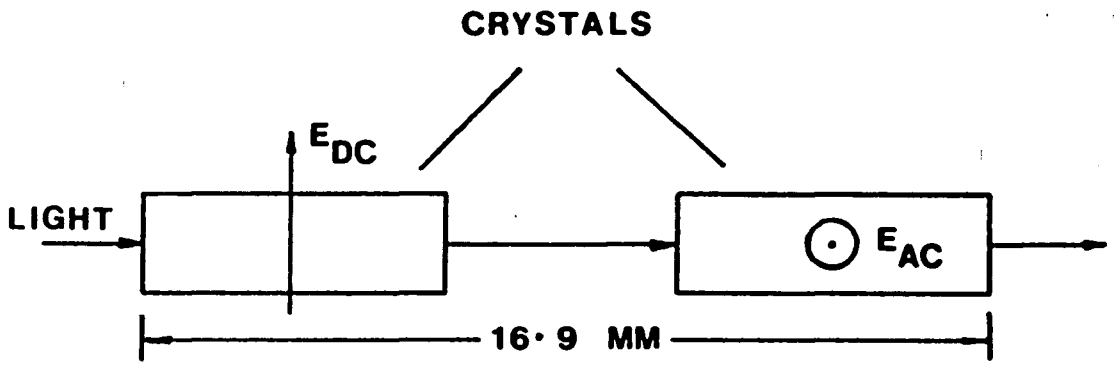

FIGURE 8 The crystals are arranged in series with the ac and dc fields applied independently.

The dimensions of each crystal are .5 by .5 by 4.2 mm and they are centered .5 inches apart. Although thin crystals are desirable to maximize modulating efficiency, a limit is imposed by the size of the laser spot image behind the telescope. The crystal's height and width have been chosen as a compromise and no problem arises at the first modulator. While this paper was in preparation, a modulator capable of handling two beams simultaneously has been constructed by Eberhardt[8]. The design does not require separate biasing and modulating crystals thus easing the problem of ray limitation. The analysis will address this case because it is of most interest at this time.

The telescope employed is a Maksutov design and may be regarded as an improved Cassegrain system[9]. The design features reduced overall length and the nearly complete absense of chromatic aber-

ations. Figure 9 is a schematic representation of this lens arrangement.

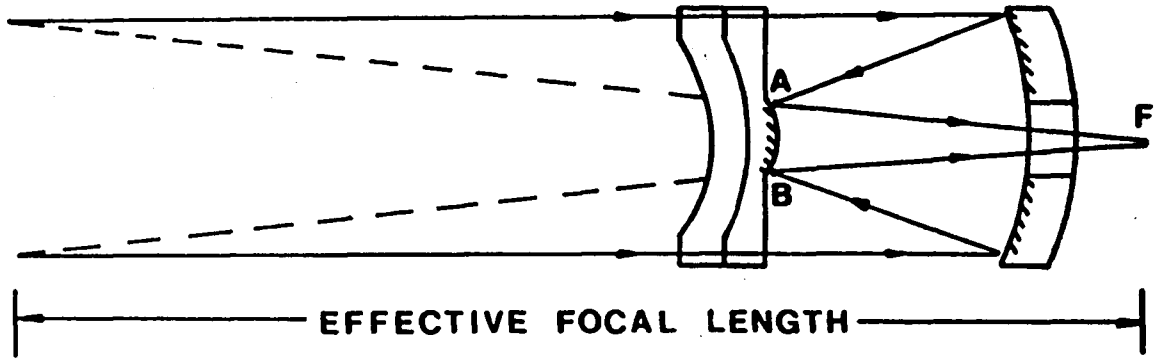

FIGURE 9 Maksutov telesope.

The effective 1 meter focal length can be obtained by extending rays $\overline{FA}$ and $\overline{FB}$ as shown, and accordingly, the telescope may be analyzed approximately as a simple lens with that focal distance. A beam expander was used to focus the laser to a spot on the target a distance Z_j away. From the fundamental Gaussian beam solution of the Maxwell equations[10], the minimum spot diameter $2\omega_o$ is given by

$$2\omega_o = \frac{4\lambda Z_j}{\pi d} \tag{18}$$

where d is the diameter of the beam at the expander (12 mm) and λ is the laser wavelength (.632μm).

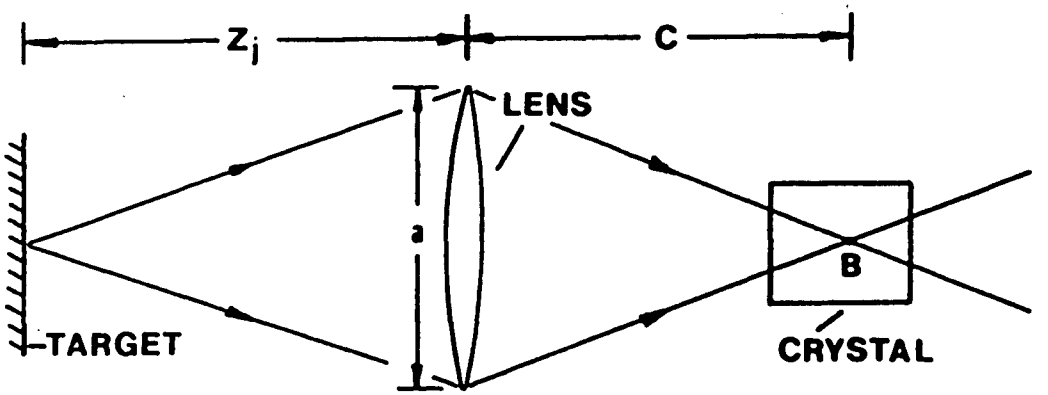

FIGURE 10 A diagram of the focusing problem with the Maksutov telescope replaced by a simple lens.

Referring to Figure 10, it is assumed that the system is initially set up with the crystal centered at point B where C is given by the formula

$$C = \frac{f\ Z_j}{Z_j - f} \tag{19}$$

and f is the focal length of the telescope. The spot's image, produced by the telescope at point B, will be reduced in size by the ratio C/Z_j. The image diameter $2\omega_o'$, obtained by combining (18) and (19), becomes

$$2\omega_o' = \frac{4\lambda\ f\ Z_j}{\pi d(Z_j - f)} \tag{20}$$

For a target distance of 8 ft this diameter is .11 mm and thus, focusing attenuation will be determined only by the rate at which the beam diverges from this minimum. Since the image location is

a function of Z_j, optimum positioning of the crystal cannot be maintained. Consider the case when the image moves an amount ΔC closer to the lens as illustrated in Figure 11.

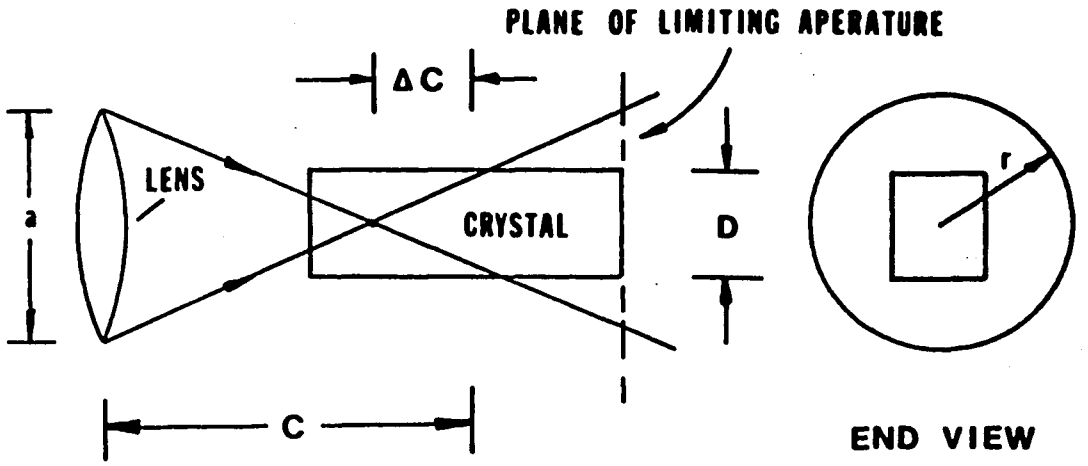

FIGURE 11 A shift in the position of the spot image causes the beam to escape from the crystal.

The limiting aperature, for this case, is the trailing face of the crystal normally referred to as the exit pupil. When the image moves away from the lens, the leading face (entrance pupil) becomes the limiting aperature. The attenuation due to pupil restrictions α_1 is defined as

$$\alpha_1 = \frac{\text{area of limiting aperature}}{\text{area of beam cross section}}$$

Once the plane of limiting aperature is known, the attenuation α_1 can be determined. In this case, α_1 is given by

$$\alpha_1 = \frac{D^2}{\pi r^2} \tag{21}$$

where the radius of the cone base r, is written in general as

$$r = \frac{a\left(\frac{L}{2} + |\Delta C|\right)}{2\,(C - \Delta C)} \tag{22}$$

The attenuation can be expressed in terms of target displacement by differentiating (19) and combining with (21) and (22) yielding

$$\alpha_1 = \frac{4D^2}{a^2\pi\left\{\frac{(Z_j - f)^2\,\frac{L}{2} + f^2(\Delta Z_j)}{(Z_j - f)\,fZ_j - f^2\,\Delta Z_j}\right\}^2} \tag{23}$$

where ΔZ_j positive indicates increasing target distance. Naturally, for values of $\alpha_1 > 1$, the attenuation is taken as 0 dB.

The target will not carry a retroreflector and therefore, the beam will scatter upon reflection. Following the suggestion of Gould and Jacobs[2], a Lambertian distribution was assumed for the reflected light intensity. Accordingly, if N_o denotes the incident

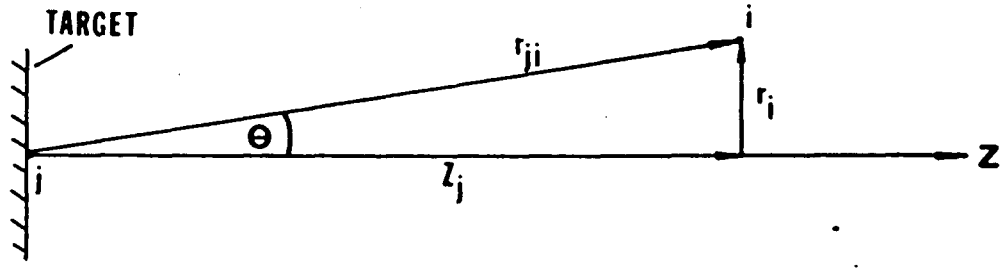

FIGURE 12 A coordinate system defining the variables needed to describe the Lambertian distribution.

power at point j on the target, as shown in Figure 12, the power density S_i at some point i away from the target can be written as

$$S_i = \frac{N' \cos \theta}{r_{ji}^2} \tag{24}$$

where r_{ji} is the distance between points j and i, θ is the plane angle formed by the vectors $\overline{r_{ji}}$ and the target normal, and N' represents a constant of proportionality. This constant may be determined knowing that the total reflected power must be γN_o where γ represents the surface reflection coefficient. Hence

$$\int_0^{2\pi} \int_0^{\infty} (S_i)\, r_i\, dr\, d\phi = \gamma\, N_o \tag{25}$$

which represents the total reflected power expressed in polar coordinates. Integration yields

$$N' = \frac{\gamma\, N_o}{2\pi} \tag{26}$$

and the reflected power density becomes

$$S_i = \frac{\gamma\, N_o}{2\pi} \cdot \frac{\cos \theta}{r_{ji}^2} \tag{27}$$

By integrating this power density over the receiver aperature, the total received power may be determined. The telescope employed utilizes multiple internal reflections to minimize physical size.

To accomplish this the aperature has an unavoidable blind spot that must be accounted for.

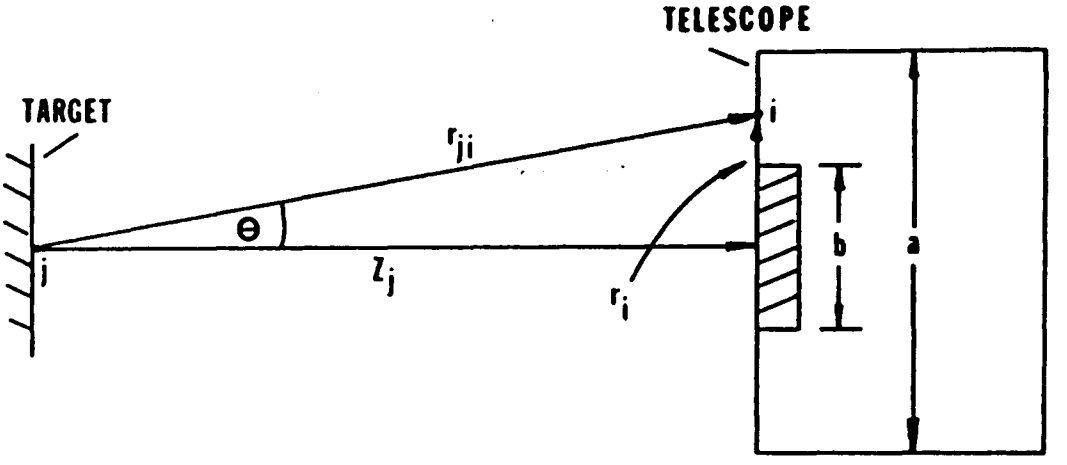

FIGURE 13 Geometry of the telescope aperature showing the effect of the blind spot.

Referring to Figure 13, the total power S_r received through the donut shaped aperature is given by

$$S_r = \int_0^{2\pi} \int_{b/2}^{a/2} \frac{\gamma N_0}{2\pi} \cdot \frac{\cos\theta}{r_{ji}^2} \, r_i \, dr \, d\phi \qquad (28)$$

where a and b represent the aperature and blind spot diameters respectively. Performing the integration and solving for the attenuation α_2 expressed as the ratio of the received power to the transmitted power yields

$$\alpha_2 = \gamma Z_j \left\{ \frac{1}{(Z_j^2 + b^2/4)^{1/2}} - \frac{1}{(Z_j^2 + a^2/4)^{1/2}} \right\} \quad (29)$$

where Z_j is the distance from the target. For target distances much greater than the aperature size

$$\alpha_2 \approx \frac{\gamma}{8} (a^2 - b^2) \frac{1}{Z_j^2} \quad (30)$$

Unfortunately, the received power Sr represents unpolarized light due to scattering occuring at the target surface. Because the details of modulator operation require linearly polarized light, an additional polarizer placed immediately before the second modulator is necessary, resulting in an additional 3 db loss in power. This loss can be absorbed in the attenuation factor now written as

$$\alpha_2 \approx \frac{\gamma}{16} (a^2 - b^2) \frac{1}{Z_j^2} \quad (31)$$

The total attenuation A_t is given by the product of α_1 and α_2 which, from (23) and (31), becomes

$$A_t = \frac{4 D^2 \delta (a^2 - b^2)}{16\pi a^2 (Z_j + \Delta Z_j)^2 \left\{ \frac{(Z_j - f)\frac{L}{2} + f^2 |\Delta Z_j|}{(Z_j - f) f Z_j - f^2 \Delta Z_j} \right\}^2} \quad (32)$$

Since α_1 is not meaningful for values greater than 1, equation (32) applies only to the case where the crystals represent the limiting

aperature. Due to practical considerations, the crystals dimensions must be chosen to minimize the microwave power necessary to achieve light modulation. Therefore, the telescope's focal length and objective size should be chosen to reduce the attenuation and its dependence upon target movement. Because α_1 and α_2 represent opposing considerations, some experimentation with (32) is necessary. Figure 14 shows the total attenuation (normalized with respect to γ) plotted against target displacement about an initial setup distance of 8 ft. Three different objective sizes have been assumed, all with 1 meter focal length. The actual objective size used was 4 in. If the initial setup distance is increased to 20 ft, as shown in Figure 15, the dependence upon target distance can be eliminated for larger displacements. Over this interval, the telescope's objective represents the limiting aperature and the attenuation is determined by (31) alone.

The available light power incident on the photomultiplier $\hat{N}_i$ may be expressed as

$$N_i = \text{(rate of photon arrival)} \cdot \text{(energy per photon)}$$

or
$$\hat{N}_i = n(t)\,\frac{hc}{\lambda} \tag{33}$$

where n(t) represents the rate of photon arrival and h is Planks constant. Solving for n(t) yields

$$n(t) = \hat{N}_i\,\frac{\lambda}{hc} \tag{34}$$

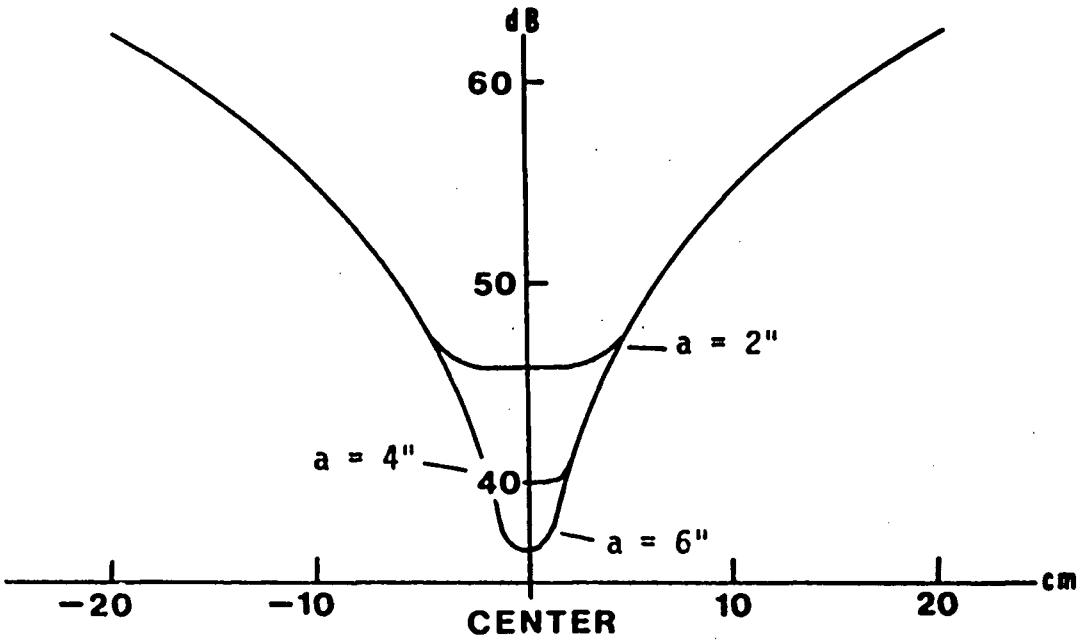

FIGURE 14 Normalized attenuation verses displacement about a center distance of 8 ft.

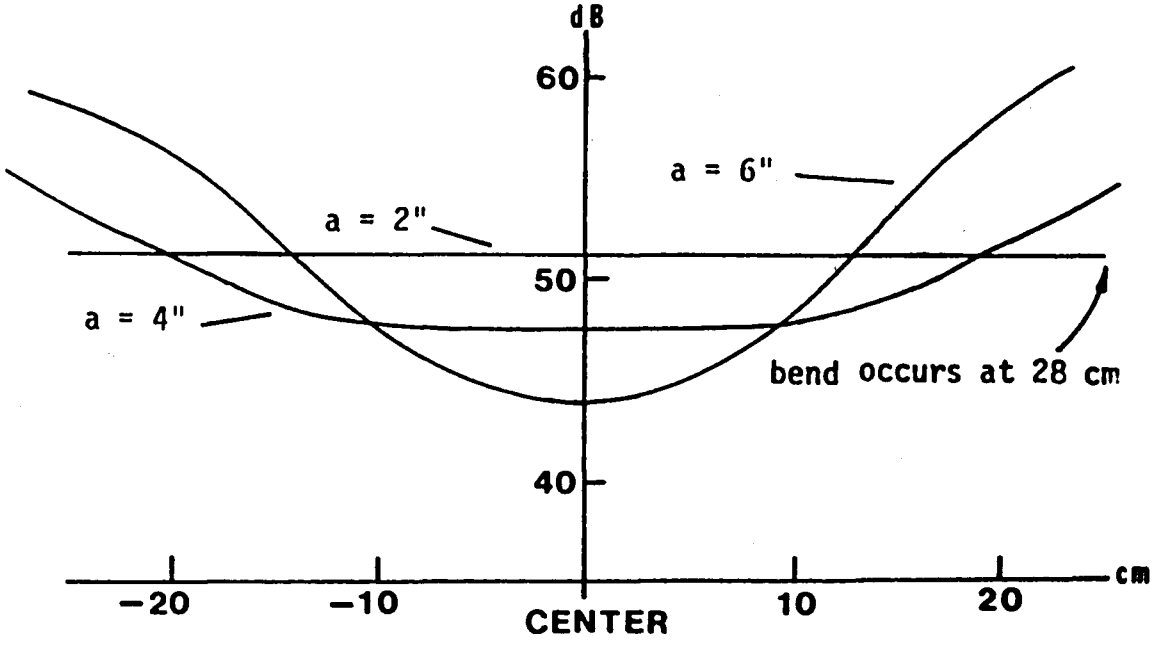

FIGURE 15 Normalized attenuation verses displacement about a center distance of 20 ft.

and if $Q(\lambda)$ is the quantum efficiency of the cathode defined as the number of electrons released from the photocathode per incident photon, then the cathode current I_k can be written as

$$I_k = n(t)\, Q(\lambda)\, e \tag{35}$$

where e is the electronic charge. From (16) and (34) it follows that

$$I_k = \frac{A_t N_o\, Q(\lambda)\, \lambda\, e}{4hc} \left\{ 1 + \frac{\mu^2}{2} \cos(\omega_1 - \omega_2)t \right\} \tag{36}$$

This induced current is amplified by secondary emission multiplication. The frequency response of the photomultiplier has been accounted for by (16) and therefore, the anode current I_A, becomes

$$I_A = G\, I_k \tag{37}$$

where G is the gain of the tube. An RCA 4463 photomultiplier was employed as the detector, and the quantum efficiency of its S-20 response at the laser's wavelength is 5-percent[11]. Assuming a laser power of 2 mW and a tube gain of 10^6 the rms anode current becomes

$$I_A = A_t \cdot (3.03 \text{ amp}) \tag{38}$$

Table III is a list of representative data taken for three different target surfaces at approximately 8 ft distance.

TABLE III

rms anode current	target material	surface reflection coefficient δ
1.6μA	reflective tape*	--
11 nA	computer card	.20
1 nA	cold black steel	.05

Substituting the above data into (38) indicates the actual attenuation constant is approximately -80 db after normalizing. This is within reasonable agreement with (32) assuming the target was displaced from center when the measurements were made. Also, separate bias and modulating crystals were still needed at that time, making the off center attenuation even larger. Since A_t represents a power ratio it is, of course, possible to increase the total received power by merely increasing the transmitted power N_o.

* Data for this case are given only for reference purposes since the analysis assumes the target is a Lambert reflector.

Noise

Light returned from the target is converted by the photomultiplier to a signal whose phase is proportional to displacement. The difficulties in measuring phase accurately stem from the presence of noise in this signal. The degree of noisiness is traditionally characterized by the signal to noise power ratio, S/N, defined as

$$\frac{S}{N} = \frac{\text{available signal power}}{\text{available noise power}}$$

This ratio can be determined for the output of the photomultiplier by considering the statistical properties of light.

The arrival of photons from a laser may be thought of as a series of impulses randomly distributed according to the Poisson distribution function.

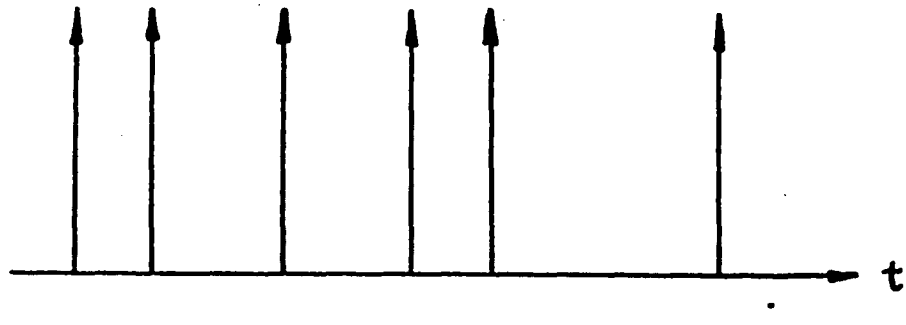

FIGURE 16 Impulses randomly distributed in time.

The probability of observing an event (arriving photon) is an interval $\{t_1, t_1 + d\tau\}$ is given by $\alpha\, d\tau$[12] where α denotes the average number of events in this interval and is given by

$$\alpha = \int_{t_1}^{t_1 + d\tau} n(t)\, d\tau \tag{39}$$

The weight of each impulse is simply the energy carried by each photon, and for a monochromatic beam this would be hc/λ. Photoelectrons released from the photocathode by the incident light carry the same statistical properties as the arriving photons[13]. Using the process shown pictorally in Figure 16 to also represent the anode current, it may be shown[14] that its power density spectrum, denoted by $S(\omega)$, is given by

$$S(\omega) = \left\{ \bar{\alpha}\, Q(\lambda)\, (Ge)^2 + S_n(\omega)\, (Q(\lambda)\, Ge)^2 \right\} \tag{40}$$

where $\bar{\alpha}$ is the time average of $n(t)$ and $S_n(\omega)$ is the spectral power density of $n(t)$. From this approach, one can view the current as consisting of a signal component and a shot noise component. Since the photomultiplier has such a large gain, the shot noise in the anode current is much larger than any thermally generated noise in the load circuit[15]. Thus, one may safely approximate the S/N ratio of the anode current to be

$$\frac{S}{N} = \frac{(Q(\lambda)\ Ge)^2 \int_{-\infty}^{\infty} S_n(\omega) \cdot H(\omega)\ d\omega}{\bar{\alpha}\ Q(\lambda)\ (Ge)^2 \int_{-\infty}^{\infty} H(\omega)\ d\omega} \tag{41}$$

where $H(\omega)$ refers to the frequency response of the instrument used to measure the current. If a bandpass filter of bandwidth Δf is used to select the difference frequency term,

$$\int_{-\infty}^{\infty} S_n(\omega)\ H(\omega)\ d\omega = \left\{ \frac{A_t\ N_o\ \lambda\ \mu^2}{8\sqrt{2}\ hc} \right\}^2 \tag{42}$$

and (41) reduces to

$$\frac{S}{N} = \frac{A_t N_o\ Q(\lambda)\ \lambda\ \mu^4}{64hc\ \Delta f} \tag{43}$$

or

$$\left[\frac{S}{N}\right] dB = 10 \log \left\{ \frac{N_o\ Q(\lambda)\ \lambda}{64hc\ \Delta f} \right\} + 10 \log\ (A_t \mu^4) \tag{44}$$

where $10 \log\ (A_t \mu^4)$ can be considered a degradation factor and it represents the loss in dB due to transmission attenuation and incomplete modulation. The measured S/N ratio, however, will be slightly lower for several reasons. Probably the most significant is that the analysis assumes any received light not passing through the demodulating crystal will not strike the photomultiplier. This extra light, if allowed to strike the photocathode,

will increase the shot noise, yet will not contribute to the IF amplitude. Secondary emmission noise in the dynode chain of the multiplier tube can reduce predicted S/N ratios by as much as 10-percent as well. Also, thermionic emission from the cathode will result in an additional noise contribution, normally referred to as dark current. According to Engstrom[16], these latter effects will not be significant for the levels of light intensity considered here.

For a filter bandwidth of 200 Hz, the S/N ratio given by (44) becomes 104 dB for 100-percent modulation and no roundtrip attenuation. Given only 50-percent modulation in each modulator, and an attenuation factor of 10^{-7}, this figure drops to 22 dB. Plots of this S/N ratio verses filter bandwidth Δf, are given in Figure 17. Various values of the degradation factor have been assumed to emphasize its effect.

Accuracy

For the purpose of establishing system accuracy, it is convenient to consider the detector output as a carrier, phase modulated with the desired distance information. Using principles from communication theory, the problem becomes that of designing a receiver capable of delivering some estimate of this phase. Estimation theory, as applied to communication system design, deals with the derivation of optimum procedures for obtaining attributes of signals within noise. The meaning of optimum must be

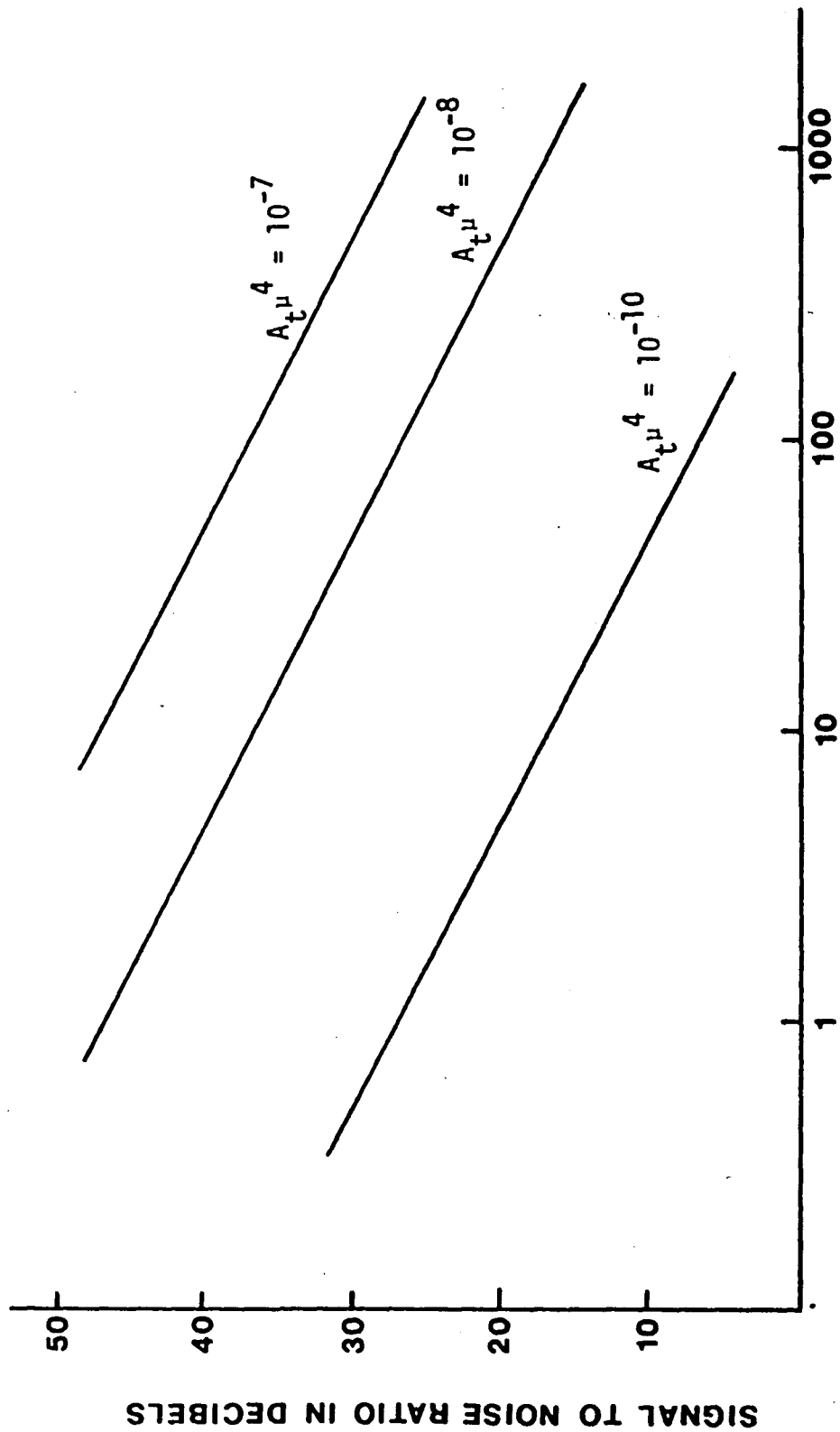

FIGURE 17 S/N ratio of photomultiplier output after bandpass filtering.

clearly defined, and for the case of estimating a continuous random variable, the accepted measure of performance has become the mean square error between the desired signal and the receiver output.

Under conditions appropriate to our case, it can be shown[17] that the optimum receiver is one that considers all allowable values of phase ϕ and chooses an estimate $\hat{\phi}$ from among them in such a way that the probability of ϕ equalling $\hat{\phi}$ is greater than the probability of ϕ equalling any other allowable value. In other words, this receiver assigns $\hat{\phi}$ the most likely value of ϕ for the given observed input, and hence is known as a maximum likelihood receiver. The criterion used most often to judge how well a particular receiver will perform is the variance of the estimated parameter. An explicit solution for the variance of $\hat{\phi}$ is difficult to obtain in this case, due to the nonlinear dependence of $\hat{\phi}$ on the input. However, Gagliardi[18] and others[19, 20] have shown that a lower bound on this variance is given by the N/S ratio at the receiver's input. Since standard deviation is a measure of uncertainty[21], the term $\sqrt{N/S}$ can be used as an indication of the relative accuracy of $\hat{\phi}$. Thus, the S/N ratio has meaning as a reciprocal distortion figure.

The accuracy of the phase measurement, and therefore the resolution of the system, can be improved by increasing the S/N ratio of the photomultiplier output. One way this can be accomplished is by decreasing the bandwidth of the filter used to se-

lect the IF frequency. Unfortunately, using this approach, the improvement in accuracy comes at the expense of measurement speed. As an example, assume that the phase of the photomultiplier output suddenly changes in response to a jump in target position. Clearly, the phase of the filtered signal cannot immediately reflect this change. Any estimate $\hat{\phi}$ produced by the receiver will be invalid until the filter reaches its steady state. To a first approximation, Ziemer[22] has estimated this delay to be $(\Delta f)^{-1}$. Recursive receiver structures have been investigated by Synder[23] and Clark[24] which produce continuously in time the best estimate $\hat{\phi}$ based on the input up to that time. It is reasonable to assume, therefore, that the overall system speed will be limited by the filter only. Plots of the maximum achievable accuracy vs filter delay are shown in Figure 18. Again various values of the degradation factor have been assumed. For applications where the speed of measurement is important, improvements in accuracy must be achieved without excessive filtering. For instance, one may seek a photomultiplier with a higher quantum efficiency at the present laser frequency, or equivalently, employ a different laser such that the quantum efficiency using the present phototube is higher. It should be emphasized that approaches to reducing the transmission attenuation factor A_t are not necessarily obvious. Probably the most efficient solution, once the trade offs have been made, is to increase the transmitted (laser) power N_o.

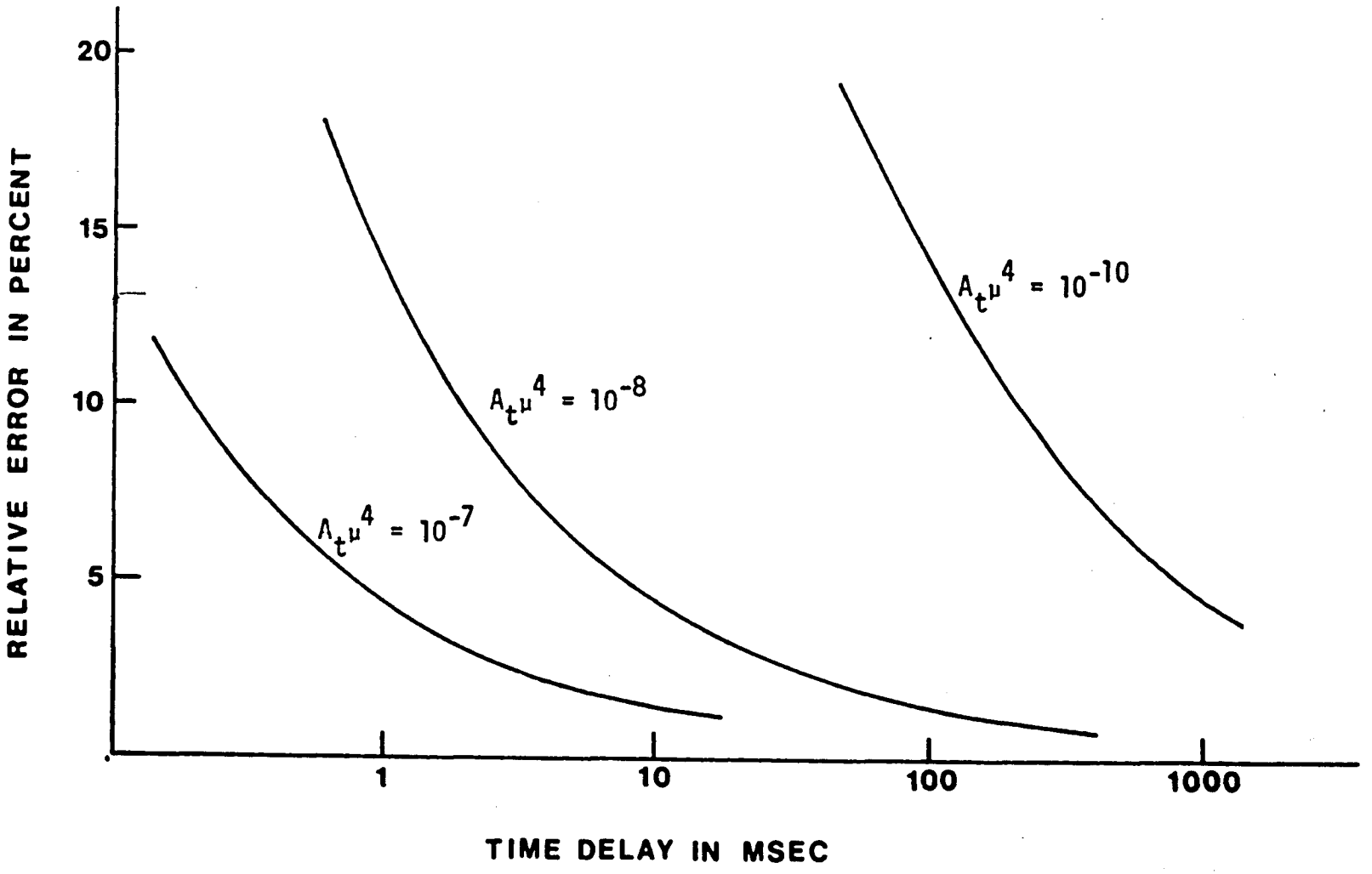

FIGURE 18 Percent error verses speed of measurement.

Conclusions

At this time, a full investigation of alternative receiver designs has not been completed. However, in order to demonstrate consistency with expected results, the filtered photomultiplier signal was fed, along with the reference signal to an oscilliscope to form a Lissajous pattern (see Figure 1B). A 360 degree phase change was observed for a target displacement of 3.8 cm. If it is assumed that the phase receiver measures shifts of up to ± 180 degrees, then to maintain a resolution of 25μm phase must be measured with an accuracy of .13-percent. This requires that the S/N ratio of the input to the phase receiver be at least 58 dB. If measurement speed is not critical, this level of performance can be approached by decreasing the filter bandwidth as discussed previously, or by averaging the estimates $\hat{\phi}$

References

1. Harvey, A. F., Coherent Light, New York: John Wiley and Sons, Inc., 1970, pp. 1259-1267.

2. Gould, G., and Jacobs, S. F., "Coherent Detection of Light Scattered From a Diffusely Reflecting Target Surface", Applied Optics, Vol. 3, No. 5, May 1964, pp. 648-649.

3. Froome, K. D. and Bradsell, R. H., "Distance Measurement by Means of a Light Ray Modulated at a Microwave Frequency", Journal of Scientific Instruments, Vol. 38, December 1961, pp. 458-462.

4. Milek, J. T. and Neuberger, M., Handbook of Electronic Materials: Linear Electrooptic Materials, Vol. 8, 1972, pp. 5-14.

5. Yariv. A., Introduction to Optical Electronics, New York: Holt, Rinehart and Winston, Inc., 1971, pp. 222-241.

6. Harvey, A. F., Coherent Light, New York: John Wiley and Sons, Inc., 1970, pp. 659-667.

7. Kaminow, I. P. and Sharpless, W. M., "Performance of $LiTaO_3$ and $LiNbO_3$ Light Modualtors at 4 GHz", Journal of Applied Optics, Vol. 6, 1967, p. 351.

8. Eberhardt, N., "Light Modulators at 4 GHz For a Continuous Wave Short Range LIDAR", A thesis by Robert T. O'Hara, Lehigh University, 1979.

9. Bauwers, A., Achievements in Optics, Amsterdam: Elsevier Publishing Company, Inc., 1946, pp. 53-59.

10. Yariv, A., Introduction to Optical Electronics, New York: Holt, Rinehart and Winston, Inc., 1971, pp. 30-35.

11. EMI Electronics Ltd. Electron Tube Division, "Photomultiplier Tubes", Brochure ref., P001, 1970.

12. Lathi, B. P., Introduction to Random Signals and Communication Theory, New York: John Wiley and Sons, Inc., 1968, pp. 191-210 and 237-240.

13. Schockly, W. and Pierce, J. R., "A Theory of Noise For Electron Multipliers", Proc. of the IRE, Vol. 26, No. 3, March 1938, p. 321.

14. Gagliardi, R. and Karp, Optical Communications, New York: John Wiley and Sons, Inc., 1976, pp. 141-155.

15. Van der Ziel, A., Noise, New York: Prentice Hall, 1954, pp. 88-119, 333-349 and 403-408.

16. Engstrom, R. W., "Multiplier Phototube Characteristics: Applications to Low Light Levels", Journal of the Optical Society of America, Vol. 37, No. 6, June 1967, pp. 420-431.

17. Wozencraft, J. M. and Jacobs, I. M., Principles of Communication Theory, New York: John Wiley and Sons, Inc., 1965, p. 212.

18. Gagliardi, R. and Karp, S., Optical Communications, New York: John Wiley and Sons, Inc., 1976, pp. 290-304.

19. Wozencraft, J. M. and Jacobs, I. M., Principles of Communication Theory, New York: John Wiley and Sons, Inc., 1965, pp. 581-591.

20. Ziemer, R. E. and Tranter, W. H., Principles of Communications: Systems Modulation and Noise, Boston: Houghton Mifflin Co., 1976, pp. 404-410.

21. Rice, S. O., "Mathematical Analysis of Random Noise", Bell System Technical Journal, Vol. 23, 1944, P. 282 and Vol. 24, 1945, P. 46.

22. Ziemer, R. E. and Tranter, W. H., Principles of Communications: Systems Modulation and Noise, Boston: Houghton Mifflin Co., 1976, pp. 66-68.

23. Synder, D. L., "Filtering and Detection for Doubly Stochastic Poisson Processes", IEEE Transaction on Information Theory, IT-18, 91, January 1972.

24. Clark, J. R., "Estimation for Poisson Processes with Applications in Optical Communications", Ph.D. Dissertation, MIT, 1971.

Vita

John Robert Regazzi was born in Madison, New Jersey on August 7, 1954 to John and Helen Regazzi. He graduated from Madison High School in 1972 and received his Bachelor of Science Degree in Electrical Engineering from Rutgers University in 1976. From 1976 to 1979, he worked at Lehigh University as a teaching assistant while studying for his Master of Science Degree, also in Electrical Engineering. John is a member of Tau Beta Pi and Eta Kappa Nu.